MATERIALS CHEMISTRY FRONTIERS

RESEARCH ARTICLE

View Article Online
View Journal

Cite this: DOI: 10.1039/d6qm00016a

Organic ionic plastic crystals composed of tetrahydrothiophenium cation with high conductivity

Keita Inoue, Yoshifumi Hirotsu, Yuko Takeoka, Masahiro Rikukawa and Masahiro Yoshizawa-Fujita *

Received 10th January 2026,
Accepted 6th March 2026

DOI: 10.1039/d6qm00016a

rsc.li/frontiers-materials

Organic ionic plastic crystals (OIPCs) are soft crystalline materials that exhibit plasticity and ionic conductivity, making them promising candidates for use as solid electrolytes. Previously, IPCs based on pyrrolidinium cations derived from the heterocyclic five-membered ring pyrrolidine have been synthesized, and their ionic conductivities have been reported. However, their performance has not yet achieved the required standard. In this study, we focused on tetrahydrothiophene, another five-membered heterocyclic compound, as a novel cationic structure. A series of novel IPCs was synthesized using tetrahydrothiophenium cations in combination with five different anions, yielding 15 compounds. Thermal analysis was conducted to determine the decomposition and phase-transition temperatures. Six of the synthesized compounds were identified as IPCs, and five were classified as ionic liquids. Among them, the compound 1-ethyltetrahydrothiophenium trifluoro(trifluoromethyl)borate ([C_2tht][CF_3BF_3]), consisting of ethyl-substituted tetrahydrothiophenium cation and CF_3BF_3 anion, exhibited an ionic conductivity of 7.19×10^{-4} S cm^{-1} at 25 °C. Notably, [C_2tht][CF_3BF_3] demonstrated an approximately one order of magnitude higher ionic conductivity at room temperature than conventional pyrrolidinium-based IPCs.

1. Introduction

Organic ionic plastic crystals (OIPCs) are soft solid compounds that possess a crystalline lattice composed of cations and anions and exhibit a certain degree of molecular-level freedom in orientation and rotation.[1] Owing to these features, OIPCs have attracted attention as next-generation solid-state electrolytes. Their non-flammability and low volatility significantly reduce the risks of leakage and combustion, making them promising candidates for use in energy storage devices, such as lithium-ion batteries, from a safety perspective.[2–4] OIPCs are being actively investigated as flexible solid electrolytes, and several studies have demonstrated that replacing liquid electrolytes with OIPCs can effectively address issues such as leakage and ignition.[5]

As solid materials with a crystalline lattice, OIPCs exhibit plasticity, that is, disorder in ion rotation or reorientation, below their melting points.[6] This enables their application as thin films to replace separators inside cells or as melt-infiltrated components in electrodes, thereby reducing interfacial resistance.[7] This melt-infiltrable property facilitates intimate contact between the electrode and electrolyte phases, thereby mitigating discontinuities in ion diffusion pathways, which are often encountered in solid electrolytes.[5,8]

In fact, all-solid-state lithium batteries employing OIPCs have demonstrated stable operation over a wide temperature range and excellent long-term cycling performance.[7,9,10] Moreover, the flexibility of OIPCs has enabled the insertion of plastic crystalline interlayers at the interface between the solid electrolyte and lithium metal anode, effectively suppressing interfacial reactions and lithium dendrite formation.[5,11]

The physical properties of OIPCs can be tuned by varying the cation–anion combinations. For example, it has been reported that the plastic-crystalline phase transition temperature and melting point can be optimized through structural modification.[12,13] OIPCs based on various cation families—such as pyrrolidinium, imidazolium, phosphonium, and sulfonium—and a wide range of anions, including PF_6^-, BF_4^-, bis(trifluoromethylsulfonyl)amide ($TFSA^-$), trifluoro(trifluoromethyl)borate ($CF_3BF_3^-$), and carbamoylcyano(nitroso)methanide ($CCNM^-$), have been widely studied.[14–19] Among them, pyrrolidinium-based IPCs have attracted particular interest because of their high chemical and thermal stabilities. Yunis *et al.* demonstrated that a variety of IPCs can be formed by combining pyrrolidinium cations with various anions and suggested that

Department of Materials and Life Sciences, Sophia University, 7-1 Kioi-cho, Chiyoda-ku, Tokyo 102-8554, Japan. E-mail: masahi-f@sophia.ac.jp

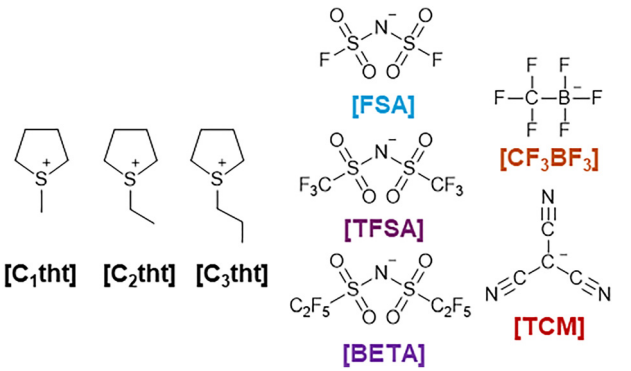

Fig. 1 Chemical structure of tetrahydrothiophenium salts with various anion species.

their structure facilitates the formation of a plastic crystal (PC) phase.[20,21] Additionally, Yamada *et al.* reported that adding lithium salts to pyrrolidinium-based IPCs further enhanced their ionic conductivity.[14] Ariga *et al.* reported that incorporating inorganic solid electrolytes enhances the thermal stability and mechanical strength of pyrrolidinium-based IPCs over a wide temperature range while maintaining high ionic conductivity.[22] Ootahara *et al.* reported that *N*,*N*-diethylpyrrolidinium trifluoro(trifluoromethyl)borate ([C_2mpyr][CF_3BF_3]) exhibits a high ionic conductivity of 1.75×10^{-4} S cm^{-1} at 25 °C.[23] These studies collectively suggest that pyrrolidinium cations offer a high degree of design freedom, facilitate the formation of IPCs, and provide high ionic conductivity. However, despite these advantages, the ionic conductivity of IPCs in the solid state and remains below the levels required for practical application.

In this study, we focused on developing new IPCs based on 1-alkyltetrahydrothiophenium cations ([$C_n$tht], n = 1–3). We synthesized 15 compounds by combining three [$C_n$tht] cations with five different anions (Fig. 1). The [$C_n$tht] cation features a five-membered heterocyclic structure similar to that of pyrrolidinium but contains only a single alkyl side chain, which enhances the cationic structural symmetry. This higher symmetry is expected to promote the formation of the IPC phases. This study aims to elucidate the relationship between molecular structure and ionic conductivity by evaluating the physicochemical properties of these [$C_n$tht]-based compounds.

2. Results and discussion

2.1. Thermal stability

Thermogravimetric analysis (TGA) was performed to evaluate the thermal stability of the synthesized compounds. TG curves are shown in Fig. S1 for all the [$C_n$tht]-based compounds synthesized in this study, and Table 1 summarizes the 5% weight loss temperatures (T_{d-5}). The T_{d-5} values of [C_1tht][FSA], [C_2tht][FSA], and [C_3tht][FSA] were 238, 244, and 260 °C, respectively, with a residual weight percentage of approximately 10%. The T_{d-5} values of [C_1tht][TFSA], [C_2tht][TFSA], and [C_3tht][TFSA] were 290, 275, and 270 °C, respectively. Similarly, [C_1tht][BETA], [C_2tht][BETA], and [C_3tht][BETA] exhibited T_{d-5} values of 286, 280, and 273 °C, respectively. In all systems with TFSA and BETA anions, the residual weight percentage at 500 °C was less than 1%.

Table 1 Comprehensive data table of phase transition behavior and thermal stability of tetrahydrothiophenium salts

Sample	T_g[a] [°C]	T_c[b] [°C]	T_{s-s}[c] [°C]	T_m[d] [°C]	ΔS_f[e] [J K^{-1} mol^{-1}]	ΔH_f[f] [kJ mol^{-1}]	T_{d-5}[g] [°C]
[C_1tht][FSA]	—	—	−17.7	232	—	23.2 (II → I)	238
[C_2tht][FSA]	—	—	0.92	82.5	104 (II → I) 9.25 (I → L)	28.4 (II → I) 3.29 (I → L)	244
[C_3tht][FSA]	—	—	—	−8.66	4.94	1.31	260
[C_1tht][TFSA]	—	—	−18.3	94.1	8.13 (III → II) 59.8 (II → I)	2.07 (III → II) 16.9 (II → I)	290
			9.91		37.2 (I → L)	13.6 (I → L)	
[C_2tht][TFSA]	—	—	−24.1	64.9	18.3 (II → I) 37.0 (I → L)	4.56 (II → I) 12.5 (I → L)	275
[C_3tht][TFSA]	—	—	−52.9 (III → II)	33.1	7.17 (III → II)	1.58 (III → II)	270
			−23.7 (II → I)		10.5 (II → I)	2.62 (II → I)	
					12.6 (I → L)	3.87 (I → L)	
[C_1tht][BETA]	—	—	—	128	29.4	11.8	286
[C_2tht][BETA]	—	—	−25.9 (IV → III)	48.0	42.4 (IV → III)	10.4 (IV → III)	280
			−15.4 (III → II)		5.74 (III → II)	1.47 (III → II)	
			10.7 (II → I)		0.45 (II → I)	0.13 (II → I)	
					32.9 (I → L)	10.6 (I → L)	
[C_3tht][BETA]	—	−18.5	6.35	18.4	68.3 (II → I) 113 (I → L)	19.1 (II → I) 33.0 (I → L)	273
[C_1tht][TCM]	—	—	17.3	104	42.6 (II → I) 29.1 (I → L)	12.6 (II → I) 11.0 (I → L)	189
[C_2tht][TCM]	—	—	—	0.74	79.5	16.5	185
[C_3tht][TCM]	−81.6	—	—	—	—	—	191
[C_1tht][CF_3BF_3]	—	—	−61.5 (III → II)	278	1.31 (III → II) 42.0 (II → I)	0.28 (III → II) 10.4 (II → I)	258
			−24.7 (II → I)				
[C_2tht][CF_3BF_3]	—	—	−72.4 (IV → III)	77.4	1.82 (IV → III)	0.36 (IV → III)	222
			−17.3 (III → II)		44.0 (III → II)	11.2 (III → II)	
			12.4 (II → I)		9.26 (II → I)	2.64 (II → I)	
					1.46 (I → L)	0.51 (I → L)	
[C_3tht][CF_3BF_3]	—	—	—	−4.90	25.8	6.91	223

[a] Glass transition temperature. [b] Crystallization temperature. [c] Solid–solid phase transition temperature. [d] Melting point. [e] Entropy of fusion. [f] Enthalpy of fusion. [g] 5% weight loss temperature.

The previously reported decomposition temperatures for [C_1tht][TFSA] and [C_2tht][TFSA] were 308 and 298 °C, respectively, which are in good agreement with those obtained in this study.[24] With the elongation of the alkyl side chain on the tetrahydrothiophenium cation, a decrease in T_{d-5} was observed. Among the structurally similar anions, FSA, TFSA, and BETA, the FSA-based salts exhibited the highest residual weight percentage. In contrast, the T_{d-5} values increased with increasing side-chain length in the FSA series, whereas the T_{d-5} values decreased with chain elongation in the TFSA and BETA series, which also exhibited low residual weight percentages.

In FSA-based OIPCs, previous studies have reported polymerization during the thermal decomposition of the FSA anion, leading to the formation of high-molecular-weight species,[25] which likely contribute to the increased residual weight percentage. The higher T_{d-5} values observed in the TFSA and BETA systems than those of FSA-based compounds are presumed to originate from the weaker basicity (*i.e.*, lower electron-donating ability) of these anions.[26] However, for pyrrolidinium and phosphonium salts bearing TFSA or BETA anions, T_{d-5} values exceeding 300 °C have been reported, which are notably higher than those of tetrahydrothiophenium-based salts.[27–29] Moreover, in sulfonium-based systems, the TFSA anion begins to decompose at approximately 280 °C.[30] These observations suggest that the S–C bond in the tetrahydrothiophenium cation is relatively weak, thermally unstable, and prone to decomposition. Furthermore, in FSA-based systems, comparing cyclic and acyclic sulfonium cations of identical molecular weight showed that the acyclic analogs tended to exhibit higher thermal stability.[31]

The T_{d-5} values of [C_1tht][TCM], [C_2tht][TCM], and [C_3tht][TCM] were 189, 185, and 191 °C, respectively, with a residual weight percentage of approximately 35–40%. Unlike the other anion systems, the TCM series showed no explicit dependency of T_{d-5} on the alkyl chain length of the tetrahydrothiophenium cation and exhibited the lowest thermal stability among the five anions investigated. As previously reported, the thermal stability of onium salts is correlated with the basicity of the anion, suggesting that the TCM anion is strongly basic. Compared to other anion systems, the TCM-based salts showed notably higher residual percentages, which can be attributed to the carbonization accompanying the thermal decomposition of the anion. The TCM anion has been reported to readily form oligomers or polymers upon heating. According to the report by Albeladi *et al.*, heating to 800 °C does not result in complete decomposition, and a residual weight of approximately 30 wt% has been observed.[32,33] This value is comparable to the yield of hydrochar obtained by hydrothermal carbonization of biomass, and the residue rate of ~40 wt% at 500 °C observed in this study is in good agreement with these findings. These results indicate that the high residual weight percentage in TCM-based OIPCs originated from carbonization during thermal degradation.

The T_{d-5} values of [C_1tht][CF_3BF_3], [C_2tht][CF_3BF_3], and [C_3tht][CF_3BF_3] were 258, 222, and 223 °C, respectively, with [C_1tht][CF_3BF_3] showing the highest thermal stability among the compounds with CF_3BF_3 anion. The dependence of T_{d-5} on the alkyl chain length was similar to that observed in the TFSA and BETA systems. The TG curves of the CF_3BF_3-based OIPCs exhibited two-step weight losses, which are presumed to be due to stepwise decomposition involving the cleavage of the $-CF_2$ groups from the anion.[34]

2.2. Phase transition behaviour

To investigate the phase-transition behavior of the OIPCs, differential scanning calorimetry (DSC) measurements were performed. Fig. 2 displays the DSC profiles for the second heating cycle for all compounds, and Table 1 summarizes the melting point (T_m), final entropy of fusion (ΔS_f), solid–solid phase transition temperature (T_{s-s}), glass transition temperature (T_g), and crystallization temperature (T_c). The temperature range from T_m to the first T_{s-s} was defined as Phase I, followed by Phases II, III, and so on.

For the compounds with FSA anions, [C_1tht][FSA] exhibited a T_{s-s} at −17.7 °C and a melting point at 232 °C; however, the ΔS_f could not be determined because of the proximity to the decomposition temperature. In the DSC measurements, the temperature range was limited to 50 °C below the decomposition temperature in order to prevent damage to the instrument. Although the measurements were conducted up to the maximum allowable temperature, no melting peak was observed in some cases. Therefore, in the figures, we extracted and presented only the temperature regions where transition peaks were clearly detected. For [C_1tht][FSA], the melting temperature was determined separately by visual observation using a melting point apparatus. In [C_2tht][FSA], a T_{s-s} was observed at 0.92 °C, with a T_m of 82.5 °C and ΔS_f of 9.25 J K^{-1} mol^{-1}, which is consistent with Timmermans' criterion. FSA-based OIPCs generally showed low ΔS_f values, likely due to the high ionic mobility in Phase I, which suppresses the entropy of fusion.[35] In [C_3tht][FSA], no T_{s-s} was observed; T_m was −8.66 °C and ΔS_f was 4.94 J K^{-1} mol^{-1}. These results suggest that [C_2tht][FSA] exhibits OIPC behavior, whereas [C_3tht][FSA], which is a liquid at room temperature, is classified as an ionic liquid (IL).

Furthermore, a comparison of the melting points of cyclic and acyclic sulfonium salts with identical molecular weights in the FSA system showed that the acyclic salts had lower melting points and were liquid at room temperature. This trend has been attributed to the larger number of accessible conformers in the liquid phase, which increases entropy and lowers melting points in ILs; five-membered ring structures possess fewer conformers than open-chain analogues.[36]

In the TFSA-based compounds, [C_1tht][TFSA] exhibited T_{s-s} at −18.3 °C and 9.91 °C, with a T_m of 94.1 °C and ΔS_f of 37.2 J K^{-1} mol^{-1}. For [C_2tht][TFSA], T_{s-s} was observed at −24.1 °C, T_m was 64.9 °C, and ΔS_f was 37.0 J K^{-1} mol^{-1}. [C_3tht][TFSA] exhibited T_{s-s} at −52.9 °C and −23.7 °C, a T_m of 33.1 °C, and ΔS_f of 12.6 J K^{-1} mol^{-1}. Reported values for [C_1tht][TFSA] include T_{s-s} at −14 °C and −16 °C and T_m at 98 °C, which are in good agreement with the present results.[24] Similarly, the reported T_{s-s} values for [C_2tht][TFSA] are −19 °C and −51 °C, with a melting point of 69 °C, again matching well with this study.[24] All the TFSA-based compounds remained

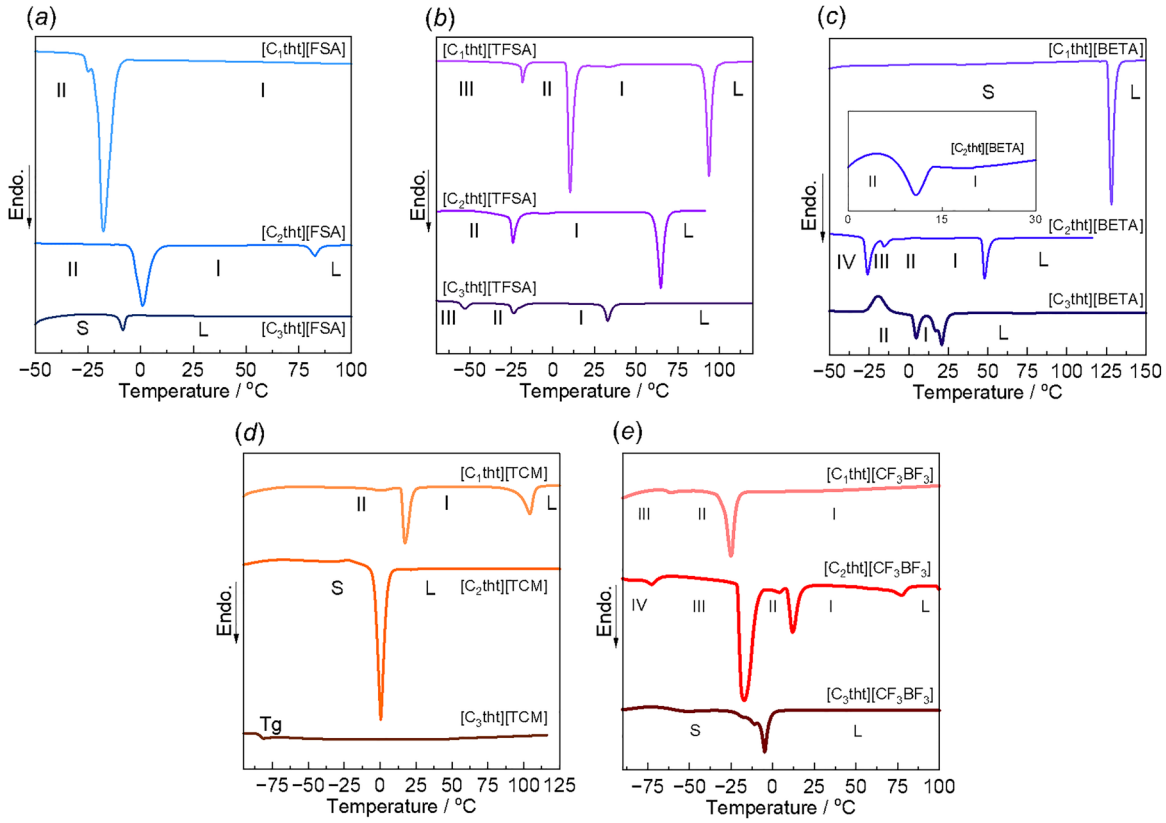

Fig. 2 DSC curves of tetrahydrothiophenium salts. (a) [$C_n$tht][FSA], (b) [$C_n$tht][TFSA], (c) [$C_n$tht][BETA], (d) [$C_n$tht][TCM], (e) [$C_n$tht][CF_3BF_3] (n = 1, 2, and 3).

solid at room temperature (25 °C) and exhibited solid–solid phase transitions. While Timmermans' criterion suggests that OIPCs typically exhibit ΔS_f values below 20 J K^{-1} mol^{-1}, all the TFSA-based compounds exceeded this threshold. However, since ionic interactions in ionic compounds tend to increase ΔS_f value, and similar trends have been reported for TFSA-containing OIPCs, these compounds are still considered to have OIPC characteristics despite their high ΔS_f values.[37]

Among the BETA-based compounds, [C_1tht][BETA] showed no T_{s-s}, with a T_m of 128 °C and ΔS_f of 29.4 J K^{-1} mol^{-1}, indicating a highly crystalline material. For [C_2tht][BETA], T_{s-s} was observed at −25.9 °C, −15.4 °C, and 10.7 °C; T_m was 48.0 °C, and ΔS_f was 32.9 J K^{-1} mol^{-1}. Although the ΔS_f value exceeded 20 J K^{-1} mol^{-1}, the behavior was similar to that of TFSA-based OIPCs, suggesting that [C_2tht][BETA] may also exhibit OIPC properties. [C_3tht][BETA] exhibited T_{s-s} at 6.35 °C, T_m of 18.4 °C, and a high ΔS_f of 113 J K^{-1} mol^{-1}. As its melting point is below room temperature, [C_3tht][BETA] exists as a liquid at room temperature and is thus classified as an IL at room temperature.

Among the TCM-based compounds, [C_1tht][TCM] exhibited T_{s-s} at 17.3 °C, a T_m of 104 °C, and ΔS_f of 29.1 J K^{-1} mol^{-1}. [C_2tht][TCM] showed no T_{s-s}, with a T_m of 0.74 °C and ΔS_f of 79.5 J K^{-1} mol^{-1}. [C_3tht][TCM] displayed only a T_g at −81.6 °C, suggesting an amorphous structure. Given that ΔS_f for [C_1tht][TCM] exceeds 20 J K^{-1} mol^{-1}, the likelihood of exhibiting OIPC behavior is low. Compared to pyrrolidinium analogs, ΔS_f was approximately 10 times higher,[38] which may be attributed to the higher orientational order of the cations in the crystal lattice. Because [C_2tht][TCM] and [C_3tht][TCM] are liquids at room temperature, they are classified as ILs.

For CF_3BF_3-based compounds, [C_1tht][CF_3BF_3] exhibited T_{s-s} at −61.5 and −24.7 °C, but no melting point was detected, making ΔS_f indeterminable. In [C_2tht][CF_3BF_3], T_{s-s} was observed at −72.4, −17.3, and 12.4 °C; T_m was 77.4 °C and ΔS_f was 1.46 J K^{-1} mol^{-1}. [C_3tht][CF_3BF_3] showed no T_{s-s}, a T_m of −4.90 °C, and ΔS_f of 25.8 J K^{-1} mol^{-1}. Notably, [C_2tht][CF_3BF_3] satisfies Timmermans' criterion and is therefore considered to have OIPC characteristics, whereas [C_3tht][CF_3BF_3], being liquid at room temperature and lacking T_{s-s}, is classified as an IL.

Based on these results, six of the 15 synthesized salts were identified as potential OIPCs: [C_1tht][TFSA], [C_2tht][X] (X = TFSA, BETA, FSA, CF_3BF_3), and [C_3tht][TFSA]. The [C_2tht] cation readily forms OIPCs with various anions. The tetrahydrothiophenium series exhibited a decrease in the melting point with increasing alkyl side-chain length, consistent with the trends observed for pyrrolidinium-based OIPCs. The [C_3tht] cation exhibited low T_m values and readily formed ILs.

2.3. Ionic conductivity

AC impedance measurements were conducted to evaluate the ionic conductivity of the tetrahydrothiophenium-based compounds. Fig. 3 shows the Arrhenius plots of the ionic

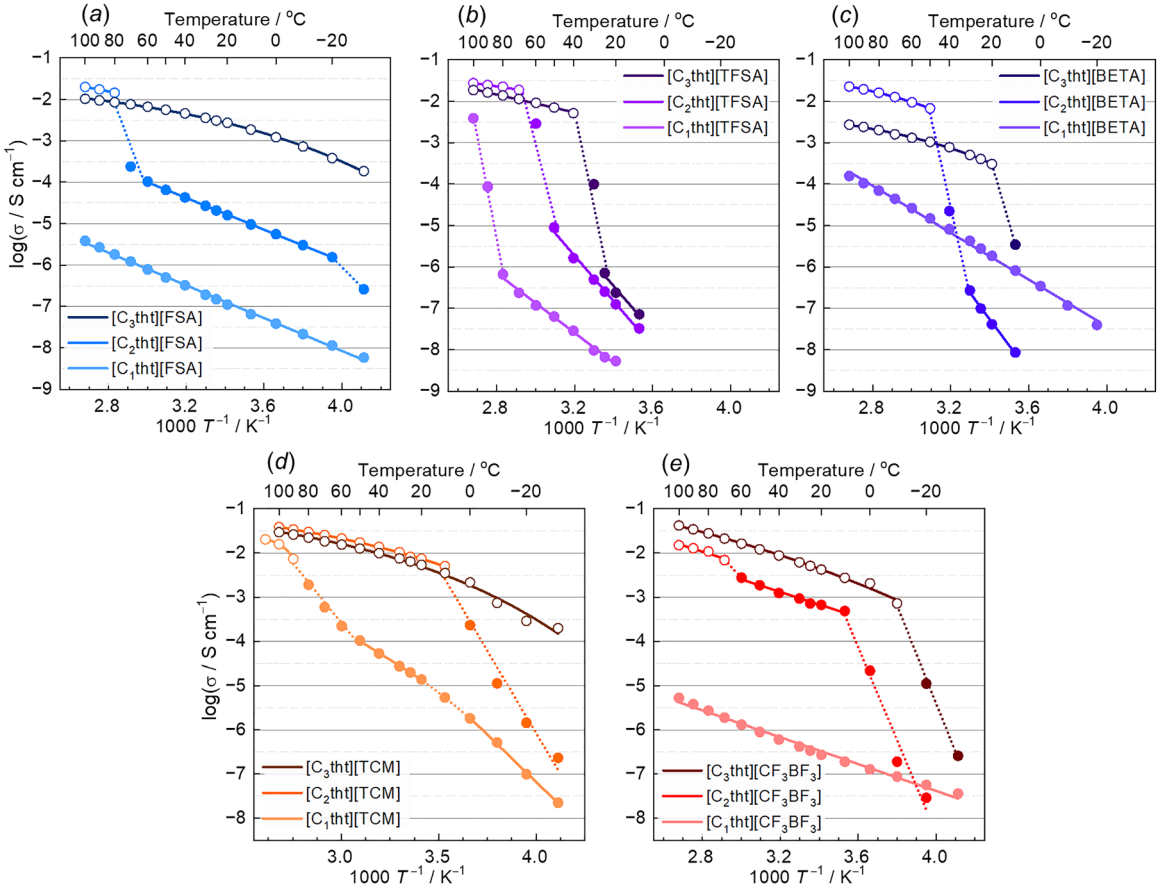

Fig. 3 Arrhenius plots of ionic conductivities for tetrahydrothiophenium salts. (a) [$C_n$tht][FSA], (b) [$C_n$tht][TFSA], (c) [$C_n$tht][BETA], (d) [$C_n$tht][TCM], (e) [$C_n$tht][CF_3BF_3] (n = 1, 2, and 3).

conductivities of all the compounds, along with their ionic conductivities at 25 °C, as summarized in Table S1. At 25 °C, the ionic conductivities of [C_1tht][FSA], [C_2tht][FSA], and [C_3tht][FSA] were 1.50×10^{-7}, 2.07×10^{-5}, and 3.09×10^{-3} S cm^{-1}, respectively. Although [C_1tht][FSA] exhibited a T_{s-s} at −17.7 °C, no significant change in conductivity was observed between −20 and −10 °C, suggesting that the structural change has a limited impact on ion mobility. For [C_2tht][FSA], conductivity changes were observed near −30 °C and 70 °C, corresponding to T_{s-s} and T_m (82.5 °C), respectively, which are consistent with the DSC results. In the Arrhenius plot of ionic conductivity for [C_3tht][FSA], no sudden change in ionic conductivity was observed around the T_m of −8.66 °C. The temperature dependence of ionic conductivity exhibited an upward convex curve, showing a Vogel–Fulcher–Tammann (VFT)-type temperature dependence. This indicates that the sample is in a liquid state and the viscosity of the liquid phase governs ion transport.[39,40] In other words, this suggests that the sample is a supercooled liquid at temperatures below the T_m.

Among FSA-based OIPCs in the solid state, the highest reported conductivity is for the pyrrolidinium-based [C_2epyr][FSA], which exhibits 1.9×10^{-5} S cm^{-1} at 30 °C.[21] In contrast, [C_2tht][FSA] developed in this study showed a higher value of 2.70×10^{-5} S cm^{-1} under the same conditions. This difference is attributed to the approximately two-fold higher ΔS_f value of [C_2epyr][FSA] compared to that of [C_2tht][FSA].

The ionic conductivities of [C_1tht][TFSA], [C_2tht][TFSA], and [C_3tht][TFSA] at 25 °C were 6.59×10^{-9}, 2.54×10^{-7}, and 7.18×10^{-7} S cm^{-1}, respectively. For [C_1tht][TFSA], [C_2tht][TFSA], and [C_3tht][TFSA], sharp decreases in conductivity were observed near 90, 60, and 30 °C, respectively, corresponding to their T_m (94.1, 64.9, and 32.9 °C), indicating significant suppression of ion mobility upon solidification. Among the TFSA-based OIPCs, the highest reported ionic conductivity at room temperature in the solid state is 2.0×10^{-6} S cm^{-1} (20 °C), exhibited by a spirocyclic quaternary ammonium salt.[41] However, the synthesis of such spirocyclic structures is often challenging due to their high molecular density, rigidity, and multistep synthesis.[42,43] In contrast, the [C_3tht][TFSA] synthesized in this study can be obtained through a simple synthetic route, offering ease of preparation. Given that the reported conductivity of a pyrrolidinium-TFSA salt is only 8.5×10^{-9} S cm^{-1} at 30 °C,[21] tetrahydrothiophenium-based salts also exhibit relatively high ionic conductivities even with the TFSA anion.

The ionic conductivities of [C_1tht][BETA], [C_2tht][BETA], and [C_3tht][BETA] at 25 °C were 3.35×10^{-6}, 9.86×10^{-8}, and 4.04×10^{-4} S cm^{-1}, respectively. The temperature dependence of

[C_1tht][BETA] followed a linear Arrhenius-type behavior without phase transitions during the measurement, consistent with its high T_m (128 °C). In contrast, [C_2tht][BETA] and [C_3tht][BETA] exhibited sharp decreases in conductivity near 40 °C and 30 °C, respectively, corresponding to their T_m (40.0 °C and 21.1 °C, respectively), indicating limited ion mobility below these temperatures. Among the BETA-based OIPCs, the highest solid-state conductivity at room temperature is reported for pyrrolidinium-based [C_2mpyr][BETA], with a value of 9.0×10^{-6} S cm^{-1}.[38] Comparison with [C_2tht][BETA] synthesized in this study reveals that [C_2mpyr][BETA] has a conductivity approximately 100 times higher, likely due to its ΔS_f value being half that of [C_2tht][BETA].

At 25 °C, the conductivities of [C_1tht][TCM], [C_2tht][TCM], and [C_3tht][TCM] were 2.00×10^{-5}, 8.19×10^{-3}, and 6.45×10^{-3} S cm^{-1}, respectively. For [C_1tht][TCM], stepwise changes were observed near 20 °C and 100 °C, corresponding to its T_{s-s} (17.6 °C) and T_m (104 °C) values, respectively. [C_2tht][TCM] exhibited a change near 0 °C, reflecting its melting point, whereas [C_3tht][TCM] exhibited a VFT-type behavior consistent with its amorphous nature and the T_g (−81.6 °C) observed in the DSC profile. The highest solid-state conductivity reported among TCM-based IPCs at room temperature is for [C_2mpyr][TCM] at 1.55×10^{-5} S cm^{-1}, which is comparable to the value observed for [C_1tht][TCM] in this study.[38] Notably, [C_1tht][TCM] also possesses a higher T_m (104 °C *vs.* 64.1 °C), indicating a broader thermal stability window, suggesting that [C_1tht][TCM] is a more promising candidate as a solid electrolyte owing to its superior ionic conductivity and thermal resilience.

The ionic conductivities of [C_1tht][CF_3BF_3], [C_2tht][CF_3BF_3], and [C_3tht][CF_3BF_3] at 25 °C were 3.39×10^{-7}, 7.19×10^{-4}, and 1.29×10^{-3} S cm^{-1}, respectively. Similar to [C_1tht][FSA], [C_1tht][CF_3BF_3] did not show a significant change near its T_{s-s} (−24.6 °C), suggesting that the ion mobility is largely unaffected by structural transitions. [C_2tht][CF_3BF_3] exhibited the highest conductivity in the solid state among all the IPCs developed in this study, implying that its molecular structure is highly favorable for ion migration. [C_3tht][CF_3BF_3] exhibited a rapid conductivity increase near −10 °C, attributed to melting at −4.90 °C, as confirmed by DSC measurement.

To our knowledge, among OIPCs, the highest solid-state conductivity at 25 °C is for [DMPyr(FH)$_2$F], a pyrrolidinium-based IPC containing HF-derived anions, with a value of 1.03×10^{-2} S cm^{-1}.[44] However, safety concerns associated with HF limit its practical applicability. The [C_2tht][CF_3BF_3] synthesized in this study demonstrated a high conductivity of 7.19×10^{-4} S cm^{-1} at 25 °C and possessed significantly better safety, indicating excellent potential as an electrolyte material. Among CF_3BF_3-based pyrrolidinium salts, the highest solid-state conductivity at room temperature is for [C_2mpyr][CF_3BF_3], with a value of 1.75×10^{-4} S cm^{-1}, suggesting that [C_2tht][CF_3BF_3] outperforms it. Two main factors may explain this superior performance. First, from a structural perspective, the tetrahydrothiophenium cation has fewer side chains than the pyrrolidinium cation, thus allowing greater rotational freedom, enhancing molecular orientation, and facilitating ion transport. Second, the ΔS_f value of [C_2mpyr][CF_3BF_3] (3.52 J K^{-1} mol^{-1}) was higher than that of [C_2tht][CF_3BF_3], implying that the latter adopted a more disordered, liquid-like structure even in the solid state.

Moreover, to evaluate molecular shape, ellipsoidality was assessed from three-dimensional molecular structures. Theellipsoidality parameters (ε_1 and ε_2) are defined as follows (Fig. S2).

$$\varepsilon_1 = b/a \quad (1)$$

$$\varepsilon_2 = c/a \quad (2)$$

where a, b, and c represent the lengths of the axes of the ellipsoid in order from longest to shortest. The ionic radii of the respective cations and anions are summarized in Table S2.

When both ε_1 and ε_2 are close to 1, the molecule is nearly spherical. As the carbon number of the cation side chain increased, the ionic radius increased, and both ε_1 and ε_2 decreased, indicating that molecular deformation toward an ellipsoidal shape was enhanced with chain elongation. This trend implies that [C_3tht]$^+$ exhibits the most pronounced deviation from spherical symmetry. Among the anions, [CF_3BF_3]$^-$ exhibited the ε_1 and ε_2 values closest to 1, indicating the highest degree of sphericity. In the comparison of ellipsoidality, the ε_1 and ε_2 values for the [C_2tht] cation were 0.27 and 0.13, respectively, whereas those for the [C_2mpyr] cation were 0.38 and 0.18. These results indicate that the [C_2tht] cation has a more ellipsoidal shape than the [C_2mpyr] cation. In contrast, the common anion CF_3BF_3 has ε_1 and ε_2 values of 0.48 and 0.46, respectively, indicating a more spherical and structurally symmetric nature. Taken together, these findings suggest that the [C_2tht][CF_3BF_3] system possesses a higher structural order than [C_2mpyr][CF_3BF_3], which contributes to the reduction in ΔS_f and enhancement of ionic conductivity. Therefore, the molecular system of [C_2tht][CF_3BF_3] is more disordered overall, contributing to its lower ΔS_f value and higher ionic conductivity. This trend is further supported by entropy partitioning of the DSC data. In [C_2tht][CF_3BF_3], the entropy associated with melting accounted for only approximately 3% of the total entropy change, indicating that the entropy change significantly increased during the solid–solid phase transitions, suggesting a higher degree of structural order in the PCs. In contrast, the ratio of ΔS_f to the total entropy change of [C_2mpyr][CF_3BF_3] was ∼28%. A smaller proportion of ΔS_f values correlates with greater disorder in the solid phase, thereby enhancing ion mobility.

Fig. 4 shows the correlation between the ratio of ΔS_f to the total entropy change and the ionic conductivity at 25 °C for both tetrahydrothiophenium- and pyrrolidinium-based compounds. The correlation coefficient between the ratio of ΔS_f to the total entropy change and the ionic conductivity was calculated to be $R^2 = 0.41$. Although the correlation coefficient was low, a clear trend was observed: a lower ΔS_f ratio corresponded to a higher ionic conductivity, implying a meaningful structure–property relationship. The dataset included only

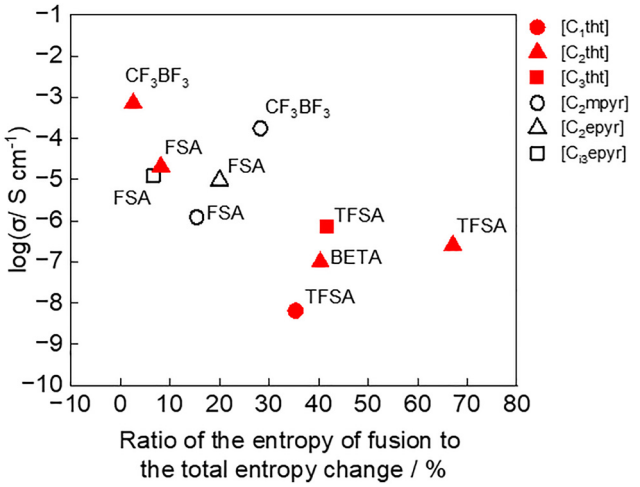

Fig. 4 Correlation between the ratio of the final entropy of fusion to the total entropy change and ionic conductivity at 25 °C for both tetrahydrothiophenium-based and pyrrolidinium-based systems. Data plotted from previous publications: open circle: *N*-ethyl-*N*-methylpyrrolidinium, open triangle: *N*,*N*-diethylpyrrolidinium, open square: *N*-ethyl-*N*-isopropylmethylpyrrolidinium.[14,23,25]

OIPCs with phase I structures at 25 °C, ensuring a consistent comparison. This correlation supports the conclusion that the high ionic conductivity of $[C_2tht][CF_3BF_3]$ results from the greater molecular freedom arising from the dissipation of the entropy of the solid–solid transition. In contrast, $[C_1tht][TFSA]$ deviated from this trend and was considered a notable exception. The DSC results suggest that $[C_1tht]$ is more prone to crystalline packing than to forming IPCs, limiting the rotational freedom and decreasing the conductivity. In addition to ΔS_f, the magnitude of the entropy at T_{s-s} may also play a role, indicating that multiple structural factors are involved.

Recently, theoretical approaches using molecular dynamics (MD) simulations have enabled the estimation of ΔS_f.[45,46] Extending such techniques to the entropies of solid–solid phase transitions may allow the prediction of ΔS_f in IPC design. Utilizing such parameters could accelerate the rational design of highly conductive IPCs. In conclusion, IPCs based on tetrahydrothiophenium cations exhibit excellent ionic conductivity and are promising candidates for the development of solid electrolytes.

2.4. Structural analysis by X-ray diffraction

To investigate the crystal structure of $[C_2tht][CF_3BF_3]$, which exhibited the highest ionic conductivity among the OIPCs obtained in this study, X-ray diffraction (XRD) measurements were conducted. Fig. 5 presents the XRD patterns of $[C_2tht][CF_3BF_3]$ in Phases I, II, III, and in the liquid phase (L). As the sample transitioned from the low-temperature to the high-temperature phase, the number of diffraction peaks decreased, consistent with the behavior previously reported for pyrrolidinium-based OIPCs.[13] At 25 °C (Phase I), the two peaks were observed at 2θ = 13.38° and 19.08°. Nishikawa *et al.* reported that $[N_{1112}][FSA]$ adopts a CsCl-type crystal structure,[47] and the XRD pattern of $[C_2tht][CF_3BF_3]$ closely resembles that of $[N_{1112}][FSA]$ (2θ = 12.93°, 18.34°), suggesting that $[C_2tht][CF_3BF_3]$ also

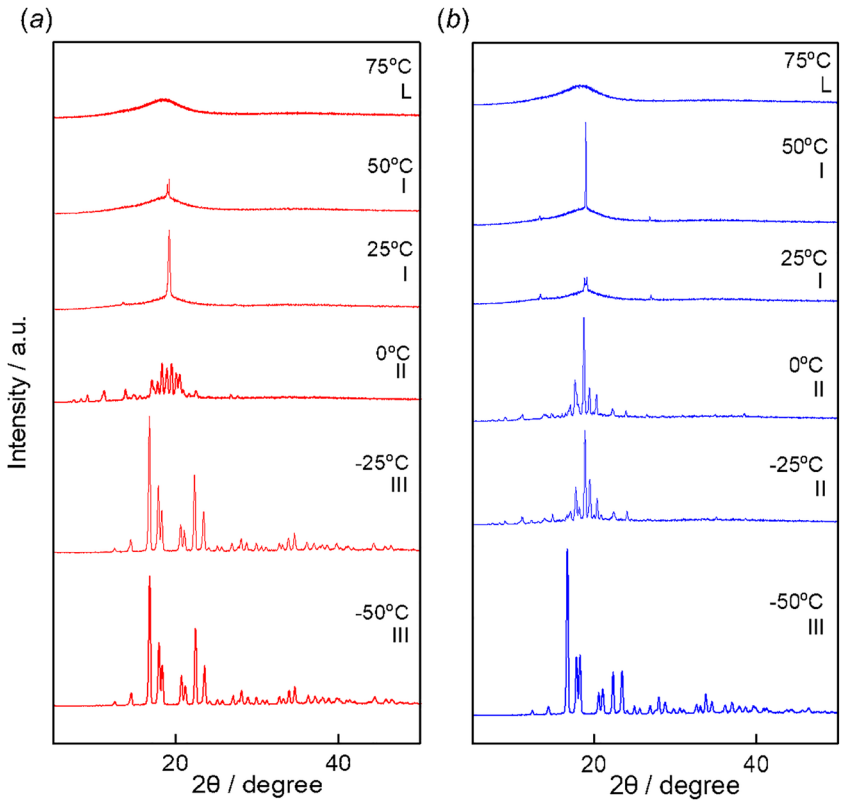

Fig. 5 X-ray diffraction patterns of $[C_2tht][CF_3BF_3]$ at phase I, II, III and L. (a) Heating, (b) cooling.

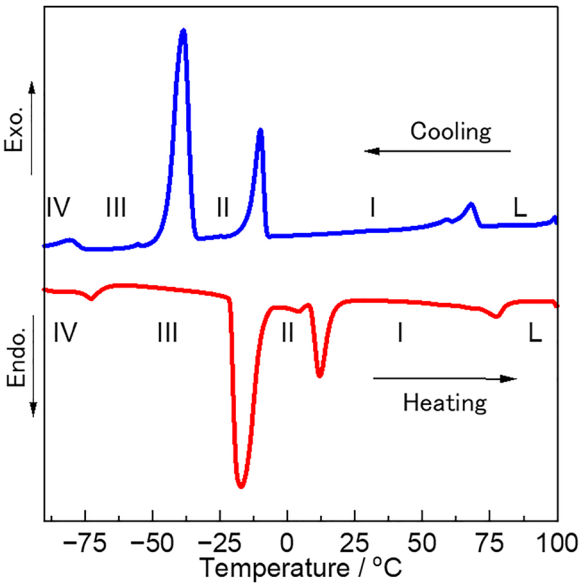

Fig. 6 DSC curves of $[C_2tht][CF_3BF_3]$ at heating and cooling scans.

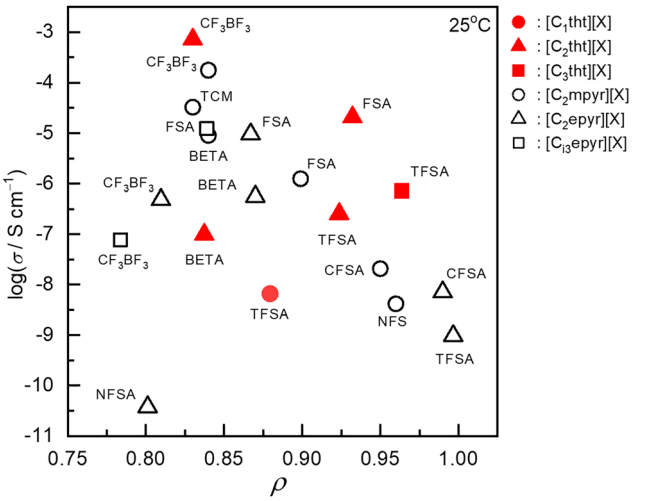

Fig. 7 Correlation between ion radius ratio (ρ) and ionic conductivity at 25 °C for both tetrahydrothiophenium-based and pyrrolidinium-based systems. Data plotted from previous publications: Open circle: *N*-ethyl-*N*-methylpyrrolidinium, open triangle: *N*,*N*-diethylpyrrolidinium, open square: *N*-ethyl-*N*-isopropylmethylpyrrolidinium.[23]

possesses a CsCl-type crystal structure. Furthermore, at −25 °C, distinct XRD patterns were observed during heating and cooling. This is consistent with the DSC results shown in Fig. 6, which indicate noticeable hysteresis between heating and cooling.

When comparing XRD patterns measured during the cooling and heating processes, the XRD patterns can sometimes be slightly different, even though they were measured at the same temperature. It has been found that the thermal history and cooling rate have a significant effect on crystallization behavior for OIPCs (in this study, the XRD patterns are shown after cooling at a rate of 50 °C min^{-1} and maintaining a constant temperature at each measurement temperature.). The detailed mechanism will be reported elsewhere.

2.5. Ionic radius ratio and ellipticity

In pyrrolidinium-based systems, prior studies have reported a negative correlation between the ionic radius ratio and ionic conductivity, with a maximum conductivity observed at a radius ratio of around 0.84.[23] In this study, we applied the same analytical approach to tetrahydrothiophenium cations, a class of sulfonium-based cations, and examined the relationship between the ionic radius ratio and ionic conductivity.

Fig. 7 presents the correlation between the ionic conductivity at 25 °C and the ionic radius ratio for both tetrahydrothiophenium- and pyrrolidinium-based systems. The ionic radius ratios of the tetrahydrothiophenium salts are summarized in Table S3. Only samples that exhibited plastic crystal (PC) phases in the solid state were included in this analysis. The results indicate that, similar to pyrrolidinium-based IPCs, tetrahydrothiophenium-based IPCs also exhibit maximum conductivity at an ionic radius ratio of approximately 0.84. This suggests a common structure–property relationship between the two cation systems. However, $[C_1tht][TFSA]$ deviated from this trend, likely because of its low probability of exhibiting IPC behavior, despite showing solid–solid transitions in the DSC profile. Overall, these findings suggest that the ionic radius ratio is a useful quantitative predictor of ionic conductivity in IPCs. Nevertheless, the actual conductivity is also strongly influenced by structural factors, such as crystallinity and the degree of molecular motion, which must be considered alongside geometric descriptors.

3. Conclusions

In this study, a series of OIPCs was synthesized using tetrahydrothiophenium cations, which are structurally analogous to five-membered pyrrolidinium cations, in combination with various anions ($TFSA^-$, $BETA^-$, FSA^-, $CF_3BF_3^-$, and TCM^-). DSC measurements identified six IPCs that remained solid at room temperature. Among them, $[C_2tht][CF_3BF_3]$ demonstrated high thermal stability and excellent electrolyte properties, with a high ionic conductivity of approximately 10^{-3} S cm^{-1} at 25 °C. Furthermore, a correlation was observed between ΔS_f and ionic conductivity, suggesting that future predictions of ΔS_f values using molecular dynamics simulations may facilitate the efficient design of high-conductivity IPC compounds. In addition, the tetrahydrothiophenium cation exhibited a similar relationship between the ionic radius ratio and ionic conductivity as previously reported for pyrrolidinium-based IPCs. This finding highlights the potential of tetrahydrothiophenium-based systems as promising candidates for developing solid-state electrolytes.

4. Experimental

4.1. Materials

Tetrahydrothiophene (>99.0%) was purchased from Tokyo Chemical Industry Co., Ltd and purified by atmospheric

distillation. Lithium bis(pentafluoroethanesulfonyl)amide (LiBETA) (>98%) and lithium bis(fluorosulfonyl)amide (LiFSA) (>98%), potassium trifluoro(methyl)borate (KCF_3BF_3) (>97%), and sodium tricyanomethanide (NaTCM) (>98%) were purchased from Tokyo Chemical Industry Co., Ltd. Celite (No. 535), activated carbon, silver nitrate, acetone, dichloromethane (super dehydrated), and acetonitrile were purchased from FUJIFILM Wako Pure Chemical Corporation. Iodomethane (>99.5%), iodoethane (>98%), and 1-iodopropane (>97%) were purchased from FUJIFILM Wako Pure Chemical Corporation and purified *via* atmospheric distillation. Lithium bis(trifluoromethylsulfonyl)amide (LiTFSA), ethanol (>99.5%) was purchased from Kanto Chemical Co. Inc.

4.2. Synthesis of 1-methyltetrahydrothiophenium iodide ([C_1tht]I)

[C_1tht]I was synthesized with reference to the reported procedure for methylated tetrahydrothiophene iodide.[24] Tetrahydrothiophene (15.5 g, 0.18 mol), purified by distillation under atmospheric pressure, was added to acetone (50 mL) along with iodomethane (25.2 g, 0.18 mol). The mixture was stirred at 60 °C for 70 h under a nitrogen atmosphere. The resulting acetone solution was poured into diethyl ether (550 mL) to induce reprecipitation. The precipitate was collected by filtration and dried under reduced pressure at 45 °C overnight, yielding a yellow powder of [C_1tht]I (30.7 g, 75% yield).

4.3. Synthesis of 1-ethyltetrahydrothiophenium iodide ([C_2tht]I)

[C_2tht]I was synthesized with reference to the reported procedure for ethylated tetrahydrothiophene iodide.[24] Tetrahydrothiophene (13.7 g, 0.16 mol), purified by distillation under atmospheric pressure, was added to acetone (25 mL) together with iodoethane (24.9 g, 0.16 mol). The mixture was stirred at 60 °C for 70 h under a nitrogen atmosphere. The resulting acetone solution was slowly added to diethyl ether (400 mL) to induce reprecipitation. The precipitate was collected by filtration and dried under reduced pressure at 45 °C overnight, yielding a yellow powder of [C_2tht]I (26.1 g, 69% yield).

4.4. Synthesis of 1-propyltetrahydrothiophenium iodide ([C_3tht]I)

[C_3tht]I was synthesized according to a previously reported procedure for ethylated tetrahydrothiophene.[24] Tetrahydrothiophene (8.42 g, 9.55×10^{-2} mol), purified by distillation under atmospheric pressure, was added to acetone (20 mL) together with iodopropane (17.9 g, 0.11 mol). The mixture was stirred at 60 °C for 70 h under a nitrogen atmosphere. The resulting acetone solution was added dropwise to diethyl ether (400 mL) to induce reprecipitation. The precipitate was collected by filtration and dried under reduced pressure at 45 °C overnight, yielding a yellow-brown liquid of [C_3tht]I (13.2 g, 53% yield).

4.5. Synthesis of 1-methyltetrahydrothiophenium bis(fluorosulfonyl)amide ([C_1tht][FSA])

The synthesis was carried out in accordance with previously reported procedures for pyrrolidinium-based salts.[14] [C_1tht]I (2.44 g, 10.6 mmol) and LiFSA (2.21 g, 11.8 mmol) were each dissolved in 5 mL of ultrapure water. The LiFSA solution was then added dropwise to the [C_1tht]I aqueous solution, and the resulting mixture was stirred at room temperature for 24 h. The reaction mixture was extracted with dichloromethane and ultrapure water (CH_2Cl_2 : H_2O = 10 : 1) after transferring the reaction mixture to dichloromethane. The absence of unreacted starting materials was confirmed using a silver nitrate test. The organic layer containing [C_1tht][FSA] was treated with activated carbon, which was subsequently removed *via* gravity filtration. The solvent was removed under reduced pressure using a rotary evaporator, and the residue was dried under vacuum at 40 °C overnight to afford a white powder of [C_1tht][FSA] (0.60 g, 20% yield). MS (FAB^+): *m*/*z* 103.1 $[M]^+$, 386.2 $[2M + X]^+$; MS (FAB^-): *m*/*z* 180.0 $[X^-]$, 463.1 $[2X + M]^-$; Anal. Calcd for $C_5H_{11}NO_4S_3F_2$: C 21.20, H 3.91, N 4.94, S 33.95; found: C 21.11, H 3.86, N 4.95, S 32.91.

4.6. Synthesis of 1-ethyltetrahydrothiophenium bis(fluorosulfonyl)amide ([C_2tht][FSA])

The synthesis was carried out in accordance with previously reported procedures for pyrrolidinium-based salts.[14] [C_2tht]I (2.46 g, 10.1 mmol) and LiFSA (2.08 g, 11.1 mmol) were each dissolved in 5 mL of ultrapure water. The LiFSA solution was then added dropwise to the [C_2tht]I aqueous solution, and the mixture was stirred at room temperature for 24 h. The reaction mixture was transferred to dichloromethane and extracted with ultrapure water (CH_2Cl_2 : H_2O = 10 : 1). The absence of unreacted starting materials was confirmed using a silver nitrate test. The organic phase containing [C_2tht][FSA] was treated with activated carbon and removed by gravity filtration. The solvent was evaporated under reduced pressure using a rotary evaporator, and the residue was dried under vacuum at 40 °C overnight to afford a white solid of [C_2tht][FSA] (2.13 g, 71% yield). MS (FAB^+): *m*/*z* 117.1 $[M]^+$, 414.2 $[2M + X]^+$; MS (FAB^-): *m*/*z* 180.0 $[X^-]$; Anal. Calcd for $C_6H_{13}NO_4S_3F_2$: C 24.24, H 4.41, N 4.71, S 32.35; found: C 24.13, H 4.31, N 4.64, S 31.58.

4.7. Synthesis of 1-propyltetrahydrothiophenium bis(fluorosulfonyl)amide ([C_3tht][FSA])

The synthesis was carried out in accordance with previously reported procedures for pyrrolidinium-based salts.[14] [C_3tht]I (2.61 g, 10.1 mmol) and LiFSA (2.08 g, 11.1 mmol) were each dissolved in 5 mL of ultrapure water. The LiFSA solution was then added dropwise to the [C_3tht]I aqueous solution, and the mixture was stirred at room temperature for 24 h. The reaction mixture was transferred to dichloromethane and extracted with ultrapure water (CH_2Cl_2 : H_2O = 10 : 1). The absence of unreacted starting materials was confirmed using a silver nitrate test. The organic phase containing [C_3tht][FSA] was treated with activated carbon and removed by gravity filtration. The solvent was evaporated under reduced pressure using a rotary evaporator, and the residue was dried under vacuum at 40 °C overnight to afford a white solid of [C_3tht][FSA] (2.13 g, 68% yield). MS (FAB^+): *m*/*z* 131.2 $[M]^+$, 442.4; MS (FAB^-): *m*/*z* 180.0 $[X^-]$, 491.2 $[2X + M]^-$; Anal. Calcd for $C_7H_{15}NO_4S_3F_2$:

C 27.00, H 4.86, N 4.50, S 30.89; found: C 26.79, H 4.87, N 4.57, S 30.27.

4.8. Synthesis of 1-methyltetrahydrothiophenium bis(trifluoromethylsulfonyl)amide ([C_1tht][TFSA])

The synthesis was carried out with reference to previously reported procedures for pyrrolidinium-based salts.[14] [C_1tht]I (1.80 g, 7.81 mmol) and LiTFSA (2.76 g, 9.61 mmol) were each dissolved in 5 mL of ultrapure water. The LiTFSA solution was then added dropwise to the [C_1tht]I aqueous solution, and the mixture was stirred at room temperature for 24 h. The resulting reaction mixture was transferred to dichloromethane and extracted with ultrapure water (CH_2Cl_2 : H_2O = 10 : 1 ratio). A silver nitrate test confirmed the absence of unreacted starting materials. The organic layer containing [C_1tht][TFSA] was treated with activated carbon and removed by gravity filtration. The solvent was removed under reduced pressure using a rotary evaporator, and the residue was dried under vacuum at 40 °C overnight to afford a yellow powder of [C_1tht][TFSA] (1.81 g, 60% yield). MS (FAB^+): *m*/*z* 103.1 $[M]^+$, 486.1 $[2M + X]^+$; MS (FAB^-): *m*/*z* 279.9 $[X^-]$, 662.9 $[2X + M]^-$; Anal. Calcd for $C_7H_{15}NO_4S_3F_6$: C 21.93, H 2.89, N 3.65, S 25.09; found: C 21.81, H 2.94, N 3.68, S 24.91.

4.9. Synthesis of 1-ethyltetrahydrothiophenium bis(trifluoromethylsulfonyl)amide ([C_2tht][TFSA])

The synthesis was carried out with reference to previously reported procedures for pyrrolidinium-based salts.[14] [C_2tht]I (1.84 g, 7.54 mmol) and LiTFSA (2.38 g, 8.30 mmol) were each dissolved in 5 mL of ultrapure water. The LiTFSA solution was then added dropwise to the [C_2tht]I aqueous solution, and the mixture was stirred at room temperature for 24 h. The resulting reaction mixture was transferred to dichloromethane and extracted with ultrapure water (CH_2Cl_2 : H_2O = 10 : 1). A silver nitrate test confirmed the absence of unreacted starting materials. The organic layer containing [C_2tht][TFSA] was treated with activated carbon and removed by gravity filtration. The solvent was removed under reduced pressure using a rotary evaporator, and the residue was dried under vacuum at 40 °C overnight to afford a yellow powder of [C_2tht][TFSA] (2.38 g, 79% yield). MS (FAB^+): *m*/*z* 117.1 $[M]^+$; MS (FAB^-): *m*/*z* 279.9 $[X^-]$, 676.8 $[2X + M]^-$; Anal. Calcd for $C_8H_{17}NO_4S_3F_6$: C 24.18, H 3.30, N 3.52, S 24.20; found: C 24.02, H 3.27, N 3.47, S 24.21.

4.10. Synthesis of 1-propyltetrahydrothiophenium bis(trifluoromethylsulfonyl)amide ([C_3tht][TFSA])

The synthesis was carried out with reference to previously reported procedures for pyrrolidinium-based salts.[14] [C_3tht]I (1.88 g, 7.29 mmol) and LiTFSA (2.30 g, 9.04 mmol) were each dissolved in 5 mL of ultrapure water. The LiTFSA solution was then added dropwise to the [C_3tht]I aqueous solution, and the mixture was stirred at room temperature for 24 h. The resulting reaction mixture was transferred to dichloromethane and extracted with ultrapure water (CH_2Cl_2 : H_2O = 10 : 1). The absence of unreacted starting materials was confirmed by a silver nitrate test. The organic layer containing [C_3tht][TFSA] was treated with activated carbon and removed by gravity filtration. The solvent was removed under reduced pressure using a rotary evaporator, and the residue was dried under vacuum at 40 °C overnight to afford a yellow powder of [C_3tht][TFSA] (2.24 g, 75% yield). MS (FAB^+): *m*/*z* 131.2 $[M]^+$, 542.3 $[2M + X]^+$; MS (FAB^-): *m*/*z* 279.9 $[X^-]$; Anal. Calcd for $C_9H_{19}NO_4S_3F_6$: C 26.28, H 3.68, N 3.40, S 23.38; found: C 26.16, H 3.69, N 3.40, S 23.16.

4.11. Synthesis of 1-methyltetrahydrothiophenium bis(pentafluoro-ethylsulfonyl)amide ([C_1tht][BETA])

The synthesis was carried out in accordance with previously reported procedures for pyrrolidinium-based salts.[14] [C_1tht]I (1.43 g, 6.21 mmol) and LiBETA (3.10 g, 8.02 mmol) were each dissolved in 5 mL of ultrapure water. The LiBETA solution was then added dropwise to the [C_1tht]I aqueous solution, and the mixture was stirred at room temperature for 24 h. The resulting reaction mixture was transferred to dichloromethane and extracted with ultrapure water (CH_2Cl_2 : H_2O = 10 : 1). The absence of unreacted starting materials was confirmed by a silver nitrate test. The organic layer containing [C_1tht][BETA] was treated with activated carbon and removed by gravity filtration. The solvent was evaporated under reduced pressure using a rotary evaporator, and the residue was dried under vacuum at 40 °C overnight to afford a white powder of [C_1tht][BETA] (1.53 g, 51% yield). MS (FAB^+): *m*/*z* 103.1 $[M]^+$, 586.2 $[2M + X]^+$; MS (FAB^-): *m*/*z* 380.0 $[X^-]$; Anal. Calcd for $C_9H_{11}NO_4S_3F_{10}$: C 22.36, H 2.29, N 2.90, S 19.90; found: C 22.31, H 2.32, N 2.95, S 19.89.

4.12. Synthesis of 1-ethyltetrahydrothiophenium bis(pentafluoro-ethylsulfonyl)amide ([C_2tht][BETA])

The synthesis was carried out with reference to previously reported procedures for pyrrolidinium-based salts.[14] [C_2tht]I (1.47 g, 6.03 mmol) and LiBETA (2.57 g, 6.63 mmol) were each dissolved in 5 mL of ultrapure water. The LiBETA solution was then added dropwise to the [C_2tht]I aqueous solution, and the mixture was stirred at room temperature for 24 h. The resulting reaction mixture was transferred to dichloromethane and extracted with ultrapure water (CH_2Cl_2 : H_2O = 10 : 1). The absence of unreacted starting materials was confirmed by a silver nitrate test. The organic layer containing [C_2tht][BETA] was treated with activated carbon and removed by gravity filtration. The solvent was evaporated under reduced pressure using a rotary evaporator, and the residue was dried under vacuum at 40 °C overnight to afford a yellow powder of [C_2tht][BETA] (2.24 g, 73% yield). MS (FAB^+): *m*/*z* 117.1 $[M]^+$; MS (FAB^-): *m*/*z* 380 $[X^-]$; for $C_{10}H_{13}NO_4S_3F_{10}$: C 24.15, H 2.63, N 2.82, S 19.34; found: C 24.11, H 2.58, N 2.73, S 19.37.

4.13. Synthesis of 1-propyltetrahydrothiophenium bis(pentafluoro-ethylsulfonyl)amide ([C_3tht][BETA])

The synthesis was carried out with reference to previously reported procedures for pyrrolidinium-based salts.[14] [C_3tht]I (1.53 g, 5.92 mmol) and LiBETA (2.60 g, 6.72 mmol) were each dissolved in 5 mL of ultrapure water. The LiBETA solution was

then added dropwise to the [C_3tht]I aqueous solution, and the mixture was stirred at room temperature for 24 h. The resulting reaction mixture was transferred to dichloromethane and extracted with ultrapure water (CH_2Cl_2 : H_2O = 10 : 1). The absence of unreacted starting materials was confirmed by a silver nitrate test. The organic layer containing [C_3tht][BETA] was treated with activated carbon and removed by gravity filtration. The solvent was evaporated under reduced pressure using a rotary evaporator, and the residue was dried under vacuum at 40 °C overnight to afford a yellow liquid of [C_3tht][BETA] (2.54 g, 84% yield). MS (FAB^+): *m*/*z* 131.2 $[M]^+$; MS (FAB^-): *m*/*z* 379.9 $[X^-]$; anal. calcd for $C_{11}H_{15}NO_4S_3F_{10}$: C 25.83, H 2.96, N 2.74, S 18.81; found: C 25.67, H 2.94, N 2.72, S 18.79.

4.14. Synthesis of 1-methyltetrahydrothiophenium tricyanomethanide ([C_1tht][TCM])

The synthesis was carried out with reference to previously reported procedures for pyrrolidinium-based salts.[38] $AgNO_3$ (2.13 g, 0.015 mol) and Na[TCM] (15.2 g, 0.13 mol) were each dissolved in ultrapure water and heated to 80 °C. The $AgNO_3$ solution was added dropwise to the Na[TCM] solution under vigorous stirring. After complete addition, the mixture was allowed to cool to room temperature and stirred for 18 h under light shielding using aluminum foil. The resulting precipitate was collected by vacuum filtration and dried under reduced pressure at 60 °C for 24 h to yield a silvery-white solid of Ag[TCM] (25.6 g, 96% yield).

[C_1tht]I (3.58 g, 15.5 mmol) and Ag[TCM] (3.38 g, 17.1 mmol) were each dissolved or dispersed in ethanol. The Ag[TCM] suspension was added dropwise to the [C_1tht]I solution, and the mixture was stirred at 40 °C for 24 h. After the reaction, AgI was removed by gravity filtration, and the filtrate was treated with activated charcoal. Ethanol was removed under reduced pressure using a rotary evaporator, and the residue was dried under vacuum at 50 °C for 24 h to afford a white powder of [C_1tht][TCM] (2.21 g, 74% yield). MS (FAB^+): *m*/*z* 103.1 $[M]^+$, 296.2 $[2M + X]^+$; MS (FAB^-): *m*/*z* 90.0 $[X^-]$, 283.2 $[2X + M]^-$; anal. calcd for $C_9H_{11}N_3S$: C 55.93, H 5.74, N 21.74, S 16.59; found: C 55.71, H 5.61, N 21.76, S 16.33.

4.15. Synthesis of 1-ethyltetrahydrothiophenium tricyanomethanide ([C_2tht][TCM])

The synthesis was carried out with reference to previously reported procedures for pyrrolidinium-based salts.[38] [C_2tht]I (3.54 g, 14.5 mmol) and Ag[TCM] (3.11 g, 15.7 mmol) were each dissolved or dispersed in ethanol. The Ag[TCM] suspension was added dropwise to the [C_2tht]I solution, and the resulting mixture was stirred at 40 °C for 24 h. After the reaction, AgI was removed by gravity filtration, and the filtrate was treated with activated carbon. Ethanol was removed under reduced pressure using a rotary evaporator, and the residue was dried under vacuum at 50 °C for 24 h to yield a yellow liquid of [C_2tht][TCM] (1.74 g, 58% yield). MS (FAB^+): *m*/*z* 117.1 [M] +, 324.3 $[2M + X]^+$; MS (FAB^-): *m*/*z* 90.0 $[X^-]$, 297.2 $[2X + M]^-$; anal. calcd for $C_{10}H_{13}N_3S$: C 57.94, H 6.32, N 20.27, S 15.47; found: C 56.67, H 6.32, N 19.78, S 15.14.

4.16. Synthesis of 1-propyltetrahydrothiophenium tricyanomethanide ([C_3tht][TCM])

The synthesis was carried out with reference to previously reported procedures for pyrrolidinium-based salts.[38] [C_3tht]I (1.74 g, 6.72 mmol) and Ag[TCM] (2.97 g, 15.0 mmol) were each dissolved or dispersed in ethanol. The Ag[TCM] suspension was added dropwise to the [C_3tht]I solution, and the resulting mixture was stirred at 40 °C for 24 h. After the reaction, AgI was removed by gravity filtration, and the filtrate was treated with activated carbon. Ethanol was removed under reduced pressure using a rotary evaporator, and the residue was dried under vacuum at 50 °C for 24 h to afford a yellow liquid of [C_3tht][TCM] (1.00 g, 67% yield). MS (FAB^+): *m*/*z* 131.2 [M] +, 352.3 $[2M + X]^+$; MS (FAB^-): *m*/*z* 90.0 $[X^-]$, 311.2 $[2X + M]^-$; anal. calcd for $C_{10}H_{13}N_3S$: C 59.70, H 6.83, N 18.99, S 14.49; found: C 58.55, H 6.85, N 18.60, S 14.44.

4.17. Synthesis of 1-methyltetrahydrothiophenium trifluoro(trifluoro-methyl)borate ([C_1tht][CF_3BF_3])

The synthesis was carried out with reference to previously reported procedures for pyrrolidinium-based salts.[23] K[CF_3BF_3] (25.4 g, 0.14 mol) was dissolved in 100 mL of acetonitrile. Separately, $AgNO_3$ (26.9 g, 0.16 mol) was added to 100 mL of acetonitrile. The two solutions were then combined and stirred at room temperature for 20 min. The resulting mixture was subjected to vacuum filtration using Celite to remove the KNO_3. The filtrate was concentrated to 20 mL using a rotary evaporator, followed by the addition of 200 mL of diethyl ether. The resulting white solid was collected by vacuum filtration and dried under reduced pressure overnight to afford a gray solid of Ag[CF_3BF_3] (16.2 g, 46% yield).

[C_1tht]I (1.92 g, 8.34 mmol) and Ag[CF_3BF_3] (2.29 g, 9.35 mmol) were each dissolved in ethanol. The [C1tht]I solution was added dropwise to the Ag[CF_3BF_3] solution, and the resulting mixture was stirred at room temperature for 24 h in the dark. After the reaction, AgI was removed by gravity filtration, and the filtrate was treated with activated carbon. Ethanol was removed under reduced pressure using a rotary evaporator, and the residue was dried under vacuum at 40 °C overnight to yield a white powder of [C_1tht][CF_3BF_3] (0.77 g, 38% yield). MS (FAB^+): *m*/*z* 103.1 $[M]^+$, 343.2 $[2M + X]^+$; MS (FAB^-): *m*/*z* 137.0 $[X^-]$, 377.1 $[2X + M]^-$; anal. calcd for $C_6H_{11}SBF_6$: C 30.03, H 4.62, S 13.36; found: C 29.80, H 4.62, S 13.44.

4.18. Synthesis of 1-ethyltetrahydrothiophenium trifluoro(trifluoro-methyl)borate ([C_2tht][CF_3BF_3])

The synthesis was carried out with reference to previously reported procedures for pyrrolidinium-based salts.[23] [C_2tht]I (1.92 g, 7.86 mmol) and Ag[CF_3BF_3] (2.08 g, 8.50 mmol) were each dissolved in ethanol. The [C_2tht]I solution was added dropwise to the Ag[CF_3BF_3] solution, and the resulting mixture was stirred at room temperature for 24 h under light shielding.

After the reaction, AgI was removed by gravity filtration, and the filtrate was treated with activated carbon. Ethanol was removed under reduced pressure using a rotary evaporator, and the residue was dried under vacuum at 40 °C overnight to yield a white viscous solid of $[C_2tht][CF_3BF_3]$ (1.07 g, 54% yield). MS (FAB^+): *m*/*z* 117.1 $[M]^+$, 371.2 $[2M + X]^+$; MS (FAB^-): *m*/*z* 137 $[X^-]$, 391.1 $[2X + M]^-$; anal. calcd for $C_7H_{13}SBF_6$: C 33.10, H 5.16, S 12.62; found: C 32.91, H 5.16, S 12.62.

4.19. Synthesis of 1-propyltetrahydrothiophenium trifluoro-(trifluoro-methyl)borate ($[C_3tht][CF_3BF_3]$)

The synthesis was carried out with reference to previously reported procedures for pyrrolidinium-based salts.[23] $[C_3tht]I$ (1.93 g, 7.47 mmol) and $Ag[CF_3BF_3]$ (2.13 g, 8.68 mmol) were each dissolved in ethanol. The $[C_3tht]I$ solution was added dropwise to the $Ag[CF_3BF_3]$ solution, and the resulting mixture was stirred at room temperature for 24 h under light shielding. After the reaction, AgI was removed by gravity filtration, and the filtrate was treated with activated carbon. Ethanol was removed under reduced pressure using a rotary evaporator, and the residue was dried under vacuum at 40 °C overnight to yield a white liquid of $[C_3tht][CF_3BF_3]$ (1.15 g, 57% yield). MS (FAB^+): *m*/*z* 131.2 $[M]^+$, 399.4 $[2M + X]^+$; MS (FAB^-): *m*/*z* 137.0 $[X^-]$, 405.2 $[2X + M]^-$; anal. calcd for $C_8H_{15}SBF_6$: C 35.84, H 5.64, S 11.96; found: C 35.54, H 5.65, S 12.07.

4.20. Identification

Compounds were identified using Fast Atom Bombardment Mass Spectrometry (FAB-MS) and proton nuclear magnetic resonance spectroscopy (^1H NMR). The NMR results are available in the Supporting Information (Fig. S3–S17). Elemental analysis was performed using a M11(J-SCIENCE LAB Co. Ltd), and scanning was performed twice.

4.21. Calculation of ionic radius and ellipsoidality by DFT

Various parameters were calculated from SMILES representations using the Descriptor Calculator, and both the ionic radius and ellipticity were determined. (DescriptorServer.ipynb - Colab)

4.22. TG-DTA measurement

Each sample was placed in an aluminum pan for measurement, and the decomposition temperature was determined using a TG-DTA7200 (Hitachi High-Tech). The measurements were carried out over a temperature range of 25 to 500 °C under a nitrogen gas flow of 200 mL min^{-1} with a heating rate of 10 °C min^{-1}.

4.23. DSC measurement

Each sample was placed in a shallow aluminum pan, and the phase transition temperatures were measured using a DSC7020 (Hitachi High-Tech). The measurement conditions were as follows: temperature range from −100 to 200 °C, nitrogen gas flow rate of 40 mL min^{-1}, and heating/cooling rate of 10 °C min^{-1}. The values of ΔH_f obtained from the DSC measurements are summarized in Table 1. ΔS_f was obtained by substituting ΔH_f and T_m, which were determined from the DSC measurements, into eqn (3).

$$\Delta S_f = \Delta H_f / T_m \quad (3)$$

4.24. AC impedance measurement

The ionic conductivity was determined by electrochemical impedance spectroscopy (EIS) using a VSP-300 electrochemical measurement system (BioLogic). Temperature control was achieved using a thermostatic chamber SU-261 (ESPEC CORP.). A doughnut-shaped spacer was fabricated using Kapton tape No. 650S-P (KENIS Co., Ltd), with an outer diameter of 16 mm, an inner diameter of 5 mm, and a thickness of 250 μm, and was affixed to an SUS electrode. Under an argon atmosphere in a glovebox, the sample was packed into the spacer opening and assembled into a coin cell to construct an evaluation cell. Measurements were conducted over a frequency range of 100 mHz to 1 MHz with an applied voltage of 10 mV. The temperature range for the measurements was −30 to 100 °C. Nyquist plots were generated from the acquired data, and the resistance values obtained through graphical analysis were used to calculate ionic conductivity. A semicircle was obtained in the Nyquist plot. The intersection with the real axis (*i.e.*, the diameter of the semicircle) was taken as the bulk resistance. The ionic conductivity was then calculated by substituting the obtained resistance value into eqn (4):

$$\sigma = d/RS \quad (4)$$

where S (S cm^{-1}) is the ionic conductivity, d (cm) is the distance between electrodes, R (Ω) is the bulk resistance, and A (cm^2) is the sectional area of the electrode.

4.25. X-ray diffraction

X-ray diffraction (XRD) profiles were obtained over the 2θ range of 1.5° to 40° with a SmartLab X-ray diffractometer (Rigaku) operating at 45 kV and 200 mA using a Ni-filtered copper target at a temperature of −50 to 75 °C.

Author contributions

Keita Inoue: conceptualization, methodology, formal analysis, investigation, resources, writing – original draft, visualization. Masafumi Hirotsu: validation, formal analysis, investigation, resources. Yuko Takeoka: data curation, supervision. Masahiro Rikuakwa: data curation, supervision. Masahiro Yoshizawa-Fujita: conceptualization, methodology, data curation, writing – review & editing, visualization, supervision, project administration, funding acquisition.

Conflicts of interest

There are no conflicts to declare.

Data availability

The data supporting this article have been included as part of the supplementary information (SI). Supplementary information: TG curves, ionic conductivity values at 25 °C, schematic diagram of ellipticity parameters, ion radius and ellipticity, ion radius ratio, ^{1}H NMR spectra. See DOI: **https://doi.org/10.1039/d6qm00016a**.

Acknowledgements

This study was supported by JSPS KAKENHI (22K19072 and 23H02072), JST-GteX (JPMJGX23S3), and a Sophia University Special Grant for Academic Research.

Notes and references

1 X. Ma, J. Yu, Y. Hu, J. Texter and F. Yan, Ionic Liquid/Poly(Ionic Liquid)-Based Electrolytes for Lithium Batteries, *Ind. Chem. Mater.*, 2023, **1**, 39–59.
2 J. C. Shin and M. Lee, Expanded Structural Design of Organic Ionic Plastic Crystals Based on Linear Tris-Pyrrolidinium Salt, *Chem. – Eur. J.*, 2025, **31**, e202500903.
3 M. Salado, T. H. Smith, N. Sirigiri, F. Chen, L. A. O'Dell, J. M. Pringle and M. Forsyth, Ammonium-Based Plastic Crystals as Solid-State Electrolytes for Lithium and Sodium Batteries, *JACS Au*, 2025, **5**, 1663–1676.
4 J. M. Pringle, P. C. Howlett, D. R. MacFarlane and M. Forsyth, Organic Ionic Plastic Crystals: Recent Advances, *J. Mater. Chem.*, 2010, **20**, 2056.
5 M. L. Thomas, K. Hatakeyama-Sato, S. Nanbu and M. Yoshizawa-Fujita, Organic Ionic Plastic Crystals: Flexible Solid Electrolytes for Lithium Secondary Batteries, *Energy Adv.*, 2023, **2**, 748–764.
6 S. Ebrahimi, S. K. Singh, A. Rhazaoui, C. Letendart, J.-C. Daigle, Y. Benabed and A. Soldera, Molecular Insights into the Structure and Dynamics of Protic Organic Ionic Plastic Crystal (OIPC) 1,7-Diazabicyclo[5.4.0]Undec-7-Ene ([DBUH])–Bis(Fluorosulfonyl)Imide ([FSI]), *J. Phys. Chem. B*, 2025, **129**, 4832–4843.
7 X. Ma, J. Yu, X. Zou, X. Wang, H. Wang, Y. Hu, M. Duan, S. Tao, S. Sun, Y. Shen and F. Yan, Electric Field-Induced Fast Li-Ion Channels in Ionic Plastic Crystal Electrolytes for All-Solid-State Batteries, *Angew. Chem., Int. Ed.*, 2025, **64**, e202505035.
8 S. Kang and H. Lee, Recent Progress of the Crystalline Organic Electrolytes for Solid-State Battery Applications, *J. Electrochem. Sci. Technol.*, 2025, **16**, 287–303.
9 B. Zhao, Q. Wang, B. Yuan, Y. Lu and X. Han, An All-Solid-State Lithium Metal Battery Based on Electrodes-Compatible Plastic Crystal Electrolyte, *Energies*, 2021, **14**, 6946.
10 X. Wang, H. Zhu, G. W. Greene, Y. Zhou, M. Yoshizawa-Fujita, Y. Miyachi, M. Armand, M. Forsyth, J. M. Pringle and P. C. Howlett, Organic Ionic Plastic Crystal-Based Composite Electrolyte with Surface Enhanced Ion Transport and Its Use in All-Solid-State Lithium Batteries, *Adv. Mater. Technol.*, 2017, **2**, 1700046.
11 Z. Li, Q. Liu, Y. Deng, M. Zhou, W. Tang, H. Dong, W. Zhao and R. Liu, In Situ Cross-Linked Plastic Crystal Electrolytes toward Superior Lithium Metal Batteries, *Mater. Today Energy*, 2023, **31**, 101198.
12 Y. Gao, Z.-N. He, W. Wei, Z.-H. Feng, Y. Qian, Z.-F. Tian and X.-M. Ren, A Superior Ionic Conducting Plastic Crystal Near Room Temperature with Electrical Bistability and Magnetic Transition, *Chem. – Eur. J.*, 2025, **31**, e202402910.
13 H. Zhou, S. Sato, Y. Nishiyama, G. Hatakeyama, X. Wang, Y. Murakami and T. Yamada, Molecular Design of Organic Ionic Plastic Crystals Consisting of Tetracyanoborate with Ultralow Phase Transition Temperature, *J. Phys. Chem. Lett.*, 2023, **14**, 9365–9371.
14 H. Yamada, Y. Miyachi, Y. Takeoka, M. Rikukawa and M. Yoshizawa-Fujita, Pyrrolidinium-Based Organic Ionic Plastic Crystals: Relationship between Side Chain Length and Properties, *Electrochim. Acta*, 2019, **303**, 293–298.
15 M. Lee, U. H. Choi, S. Wi, C. Slebodnick, R. H. Colby and H. W. Gibson, 1,2-Bis[N-(N′-Alkylimidazolium)]Ethane Salts: A New Class of Organic Ionic Plastic Crystals, *J. Mater. Chem.*, 2011, **21**, 12280.
16 H. Amir, M. Kar, L. A. O'Dell, M. Forsyth, M. Swadźba-Kwaśny and J. D. Holbrey, New Tetrabutylphosphonium Organic Ionic Plastic Crystals Incorporating Borate Anions, *J. Mater. Chem. A*, 2025, **13**, 18842–18850.
17 M. Anouti, L. Timperman, M. El Hilali, A. Boisset and H. Galiano, Sulfonium Bis(Trifluorosulfonimide) Plastic Crystal Ionic Liquid as an Electrolyte at Elevated Temperature for High-Energy Supercapacitors, *J. Phys. Chem. C*, 2012, **116**, 9412–9418.
18 A. Sourjah, C. S. M. Kang, F. M. Ferrero Vallana, O. E. Hutt, L. A. O'Dell and J. M. Pringle, Investigation of the Benefits of the Oxazolidinium Cation for Plastic Crystal and Ionic Liquid Electrolytes, *Front. Batter. Electrochem.*, 2024, **3**, 1330604.
19 J. Janikowski, M. R. Razali, C. M. Forsyth, K. M. Nairn, S. R. Batten, D. R. MacFarlane and J. M. Pringle, Physical Properties and Structural Characterization of Ionic Liquids and Solid Electrolytes Utilizing the Carbamoylcyano-(Nitroso)Methanide Anion, *ChemPlusChem*, 2013, **78**, 486–497.
20 L. M. McGrath and J. F. Rohan, Pyrrolidinium Containing Ionic Liquid Electrolytes for Li-Based Batteries, *Molecules*, 2020, **25**, 6002.
21 R. Yunis, T. W. Newbegin, A. F. Hollenkamp and J. M. Pringle, Ionic Liquids and Plastic Crystals with a Symmetrical Pyrrolidinium Cation, *Mater. Chem. Front.*, 2018, **2**, 1207–1214.
22 K. Ariga, S. Akakabe, R. Sekiguchi, M. L. Thomas, Y. Takeoka, M. Rikukawa and M. Yoshizawa-Fujita, Boosting the Ionic Conductivity of Pyrrolidinium-Based Ionic Plastic Crystals by LLZO Fillers, *ACS Omega*, 2024, **9**, 22203–22212.
23 T. Ootahara, K. Hatakeyama-Sato, M. L. Thomas, Y. Takeoka, M. Rikukawa and M. Yoshizawa-Fujita, Efficient Exploration of Highly Conductive Pyrrolidinium-Based Ionic Plastic Crystals Using Materials Informatics, *ACS Appl. Electron. Mater.*, 2024, **6**, 5866–5878.

24 Q. Zhang, S. Liu, Z. Li, J. Li, Z. Chen, R. Wang, L. Lu and Y. Deng, Novel Cyclic Sulfonium-Based Ionic Liquids: Synthesis, Characterization, and Physicochemical Properties, *Chem. – Eur. J.*, 2009, **15**, 765–778.

25 J. Huang and A. F. Hollenkamp, Thermal Behavior of Ionic Liquids Containing the FSI Anion and the Li^+ Cation, *J. Phys. Chem. C*, 2010, **114**, 21840–21847.

26 T. Mandai, K. Yoshida, K. Ueno, K. Dokko and M. Watanabe, Criteria for Solvate Ionic Liquids, *Phys. Chem. Chem. Phys.*, 2014, **16**, 8761.

27 B. Siu, C. G. Cassity, A. Benchea, T. Hamby, J. Hendrich, K. J. Strickland, A. Wierzbicki, R. E. Sykora, E. A. Salter, R. A. O'Brien, K. N. West and J. H. Davis, Thermally Robust: Triarylsulfonium Ionic Liquids Stable in Air for 90 Days at 300 °C, *RSC Adv.*, 2017, **7**, 7623–7630.

28 K. Tsunashima and M. Sugiya, Physical and Electrochemical Properties of Low-Viscosity Phosphonium Ionic Liquids as Potential Electrolytes, *Electrochem. Commun.*, 2007, **9**, 2353–2358.

29 N. Papaiconomou, J. Salminen, J.-M. Lee and J. M. Prausnitz, Physicochemical Properties of Hydrophobic Ionic Liquids Containing 1-Octylpyridinium, 1-Octyl-2-Methylpyridinium, or 1-Octyl-4-Methylpyridinium Cations, *J. Chem. Eng. Data*, 2007, **52**, 833–840.

30 A. J. R. Rennie, V. L. Martins, R. M. Torresi and P. J. Hall, Liquids Containing Sulfonium Cations as Electrolytes for Electrochemical Double Layer Capacitors, *J. Phys. Chem. C*, 2015, **119**, 23865–23874.

31 H.-B. Han, J. Nie, K. Liu, W.-K. Li, W.-F. Feng, M. Armand, H. Matsumoto and Z.-B. Zhou, Ionic Liquids and Plastic Crystals Based on Tertiary Sulfonium and Bis(Fluorosulfonyl)Imide, *Electrochim. Acta*, 2010, **55**, 1221–1226.

32 Z. Chen, S. Pronkin, T.-P. Fellinger, K. Kailasam, G. Vilé, D. Albani, F. Krumeich, R. Leary, J. Barnard, J. M. Thomas, J. Pérez-Ramírez, M. Antonietti and D. Dontsova, Merging Single-Atom-Dispersed Silver and Carbon Nitride to a Joint Electronic System *via* Copolymerization with Silver Tricyanomethanide, *ACS Nano*, 2016, **10**, 3166–3175.

33 N. Albeladi, L. S. Blankenship and R. Mokaya, Ultra-High Surface Area Ionic-Liquid-Derived Carbons That Meet Both Gravimetric and Volumetric Methane Storage Targets, *Energy Environ. Sci.*, 2024, **17**, 3060–3076.

34 Z.-B. Zhou, H. Matsumoto and K. Tatsumi, Low-Melting, Low-Viscous, Hydrophobic Ionic Liquids: 1-Alkyl(Alkyl Ether)-3-Methylimidazolium Perfluoroalkyltrifluoroborate, *Chem. – Eur. J.*, 2004, **10**, 6581–6591.

35 R. Yunis, A. F. Hollenkamp, C. Forsyth, C. M. Doherty, D. Al-Masri and J. M. Pringle, Organic Salts Utilising the Hexamethylguanidinium Cation: The Influence of the Anion on the Structural, Physical and Thermal Properties, *Phys. Chem. Chem. Phys.*, 2019, **21**, 12288–12300.

36 Y. K. J. Bejaoui, F. Philippi, H.-G. Stammler, K. Radacki, L. Zapf, N. Schopper, K. Goloviznina, K. A. M. Maibom, R. Graf, J. A. P. Sprenger, R. Bertermann, H. Braunschweig, T. Welton, N. V. Ignat'ev and M. Finze, Insights into Structure–Property Relationships in Ionic Liquids Using Cyclic Perfluoroalkylsulfonylimides, *Chem. Sci.*, 2023, **14**, 2200–2214.

37 S. Forsyth, J. Golding, D. R. MacFarlane and M. Forsyth, N-Methyl-N-Alkylpyrrolidinium Tetrafluoroborate Salts: Ionic Solvents and Solid Electrolytes, *Electrochim. Acta*, 2001, **46**, 1753–1757.

38 S. Yamaguchi, H. Yamada, Y. Takeoka, M. Rikukawa and M. Yoshizawa-Fujita, Synthesis of Pyrrolidinium-Based Plastic Crystals Exhibiting High Ionic Conductivity at Ambient Temperature, *New J. Chem.*, 2019, **43**, 4008–4012.

39 H. Tokuda, K. Hayamizu, K. Ishii, Md. A. B. H. Susan and M. Watanabe, Physicochemical Properties and Structures of Room Temperature Ionic Liquids. 1. Variation of Anionic Species, *J. Phys. Chem. B*, 2004, **108**, 16593–16600.

40 K. Hayamizu, Direct Relations between Ion Diffusion Constants and Ionic Conductivity for Lithium Electrolyte Solutions, *Electrochim. Acta*, 2017, **254**, 101–111.

41 Y. Abu-Lebdeh, E. Austin and I. J. Davidson, Spiro-Ammonium Imide Salts as Electrolytes for Lithium Batteries., *Chem. Lett.*, 2009, **38**(8), 783.

42 N. Derkach, K. Levchenko, I. Iermolenko, E. Ostapchuk, D. Lega, V. Makhankova, A. Rozhenko, D. Volochnyuk and S. Ryabukhin, Efficient multigram synthesis of 3,3-spiro-α-proline containing chimeras, 2024, preprint.

43 M. Waser, K. Gratzer, R. Herchl and N. Müller, Design, Synthesis, and Application of Tartaric Acid Derived N-Spiro-quaternary Ammonium Salts as Chiral Phase-Transfer Catalysts, *Org. Biomol. Chem.*, 2012, **10**, 251–254.

44 R. Taniki, K. Matsumoto, R. Hagiwara, K. Hachiya, T. Morinaga and T. Sato, Highly Conductive Plastic Crystals Based on Fluorohydrogenate Anions, *J. Phys. Chem. B*, 2013, **117**, 955–960.

45 M. H. Keshavarz, A. R. Akbarzadeh, R. Rahimi, M. Jafari, M. Pasandideh and R. Sadeghi, A Reliable Method for Prediction of Enthalpy of Fusion in Energetic Materials Using Their Molecular Structures, *Fluid Phase Equilib.*, 2016, **427**, 46–55.

46 T. Endo, K. Sunada, H. Sumida and Y. Kimura, Origin of Low Melting Point of Ionic Liquids: Dominant Role of Entropy, *Chem. Sci.*, 2022, **13**, 7560–7565.

47 K. Nishikawa, T. Yamada, K. Fujii, H. Masu, K. Tozaki and T. Endo, Formulation of Diffraction Intensity of Ionic Plastic Crystal and Its Application to Trimethylethylammonium Bis(Fluorosulfonyl)Amide, *Bull. Chem. Soc. Jpn.*, 2021, **94**, 2011–2018.

